Frontiers in Heat and Mass Transfer

Tech Science Press

DOI: 10.32604/fhmt.2024.058274

ARTICLE

Molecular Dynamics Study on Hydrothermal Response of PNIPAM: From Single Chain to Cross-Linked Polymer

Xianzhi Chen[1], Dong Niu[1,*], Hongtao Gao[1] and Mu Du[2,3,*]

[1]Institute of Refrigeration & Cryogenics Engineering, Dalian Maritime University, Dalian, 116026, China

[2]Institute for Advanced Technology, Shandong University, Jinan, 250061, China

[3]Shenzhen Research Institute of Shandong University, Shandong University, Shenzhen, 518057, China

*Corresponding Authors: Dong Niu. Email: niudong@dlmu.edu.cn; Mu Du. Email: dumu@sdu.edu.cn

Received: 09 September 2024 Accepted: 15 October 2024 Published: 19 December 2024

ABSTRACT

Thermosensitive hydrogel can integrate vapor molecular capture, *in-situ* liquefaction, and thermal-induced water release for freshwater capture. This study aimed to examine the dynamic behavior of poly (N-isopropylacrylamide) (PNIPAM) single chain and cross-linking thermosensitive hydrogel through molecular dynamics simulation. Specifically, the impact of lower critical solution temperature (LCST) on the conformation of polymer chain and the interaction between water and polymer chain were also investigated. The polymer chain conformation underwent a transition from coil to globule when the temperature exceeded the LCST, indicating the temperature responsiveness of PNIPAM. Additionally, thermosensitive hydrogel samples with different cross-linking degrees (DOC) were studied, and relevant parameters such as the number of free water, the diffusion coefficient of water, and the pore size distribution were counted to evaluate the temperature responsiveness and water release characteristics of thermosensitive hydrogel.

KEYWORDS

Thermosensitive hydrogel; water harvesting; coil to globule; cross-linked; molecular dynamics simulation

1 Introduction

Freshwater resources have increasingly attracted global attention. Ghasemi et al. [1] proposed solar thermal evaporation technology based on local heating for water desalination. The utilization of photothermal materials to achieve direct desalination of seawater is suitable for the needs of modern society due to their energy efficiency, reduced resource consumption, utilization of low-grade energy sources, and preservation of water security. Numerous studies have been recently conducted on photothermal materials, evaporator optimization design, and arrangement form for the development of solar thermal seawater desalination systems. These findings indicate that the inefficiency of the condensing component significantly hinders the overall efficiency of the solar thermal seawater desalination system [2,3]. When employing the traditional transparent cover plate used as condensing components, four factors impede further enhancement of water collection performance. Firstly, the condensation droplets reduce the light transmittance of the cover plate [4]. Second, the low intrinsic

thermal conductivity (<5 $W \cdot m^{-1} \cdot K^{-1}$) of transparent cover plates, such as glass, leads to a significant thermal resistance during the vapor condensation heat transfer process [5]. Third, increased latent heat and light absorption reduce the heat transfer temperature difference of the upper transparent cover plate, thus decreasing the driving force for condensation [6]. Furthermore, a large amount of non-condensable gas in the photothermal desalination system significantly decreases the condensation heat transfer coefficient [7,8]. Therefore, the optimization of the condensing component is the key to improve the overall efficiency of desalination system.

Hydrogel is a hydrophilic but insoluble polymer network, which can quickly swell and absorb a large amount of water. Hydrogels have been widely used in diverse fields, including histological engineering [9], targeted therapy [10], desalination [11], soft electronics [12], and selective protein [13]. Compared with traditional glass cover plates in non-condensing situations, gel materials for air freshwater capture in low relative humidity conditions [14–17] has demonstrated superior performance. Certain hydrogels demonstrate swift reactivity to external stimuli, as seen in thermosensitive hydrogels composed of polymer chains and water that enable water release upon reaching a critical temperature. Upon exceeding this critical temperature, the polymer network undergoes a transition to an opaque state, resulting in light modulation dependent on temperature. Based on the photoregulation of poly (N-isopropylacrylamide) (PNIPAM), Yu et al. [18] integrated modified MXene nanoparticles, and Ni-Ti shape memory alloy (SMA) to give intelligent Windows heat storage, temperature control and ventilation functions. Thermosensitive hydrogels possessing attributes such as flexibility, transparency, temperature responsiveness, and water release capabilities are thus deemed appropriate for integration as condensing elements in solar thermal desalination systems.

PNIPAM [19] is considered a promising thermosensitive hydrogel due to its unique properties, including the lower critical solution temperature (LCST) of approximately 305 K in aqueous environments. When exposed to temperature changes, PNIPAM undergoes a phase separation process in its aqueous solution, leading to a conformational transition from coil to globule. This behavior causes the PNIPAM hydrogel to absorb a significant amount of water at temperatures below the LCST, release a portion of the absorbed water at temperatures above the LCST, and ultimately collapse [20]. Numerous researchers have conducted comprehensive simulation studies on PNIPAM polymer chains [21–25]. Simple polymers consist of elongated chains of monomers connected by hydrogen bonding and steric hindrance. The three-dimensional configuration of hydrogels is strengthened through the incorporation of cross-linking agents to bolster the stability of the hydrogel, leading to a more robust structure. In the realm of polymer science, physical cross-linking represents a tenuous connection between specific domains, while chemical cross-linking is the formation of stable covalent bonds between polymer chains and cross-linkers [26–29]. The investigation of cross-linked hydrogels in experimental settings presents numerous challenges stemming from varying synthesis parameters, including the degree of cross-linking (DOC) and water content [30,31]. All-atom molecular dynamics (MD) simulations, however, offer a valuable tool for supplementing empirical observations and facilitating a deeper understanding of the significant impacts of chemical cross-linking type, DOC and water content on the structural properties of these materials [32].

There are several studies on hydrogels by MD simulation, with a predominant emphasis on the mechanical and deformation properties of these materials [33–36]. Tamai et al. [37] conducted simulations to investigate the influence of water-polymer interaction in three hydrogels, examining the relationship between hydrogen bond distribution, water content, and temperature, as well as determining the hydrophilicity trend of these hydrogels. Additionally, the concentration dependence of volume phase transitions in high-density PNIPAM microgel suspension was found to be consistent with macroscopic values [38]. Lehmann et al. [39] studied on the impact of various cross-linkers on

PNIPAM thermosensitive hydrogels. The findings indicated that while the cross-linker did not significantly alter the initial temperature of LCST, it did influence the degree of expansion and distribution of pore sizes. Further, the effects of different cross-linking agents on the swelling behavior of hydrogels have been investigated [40,41], and the results show that the microgels cross-linked with ethylene glycol and triethylethylene glycol dimethacrylate exhibit significant swelling behavior near LCST, while the microgels cross-linked with N, N'-methylene diacrylamide (BIS) exhibit reduced volume changes. Previous simulation study [42] has illustrated the substantial water release of PNIPAM thermosensitive hydrogel through the MD simulation of the channel graft of PNIPAM.

The attributes of water absorption, water release, and temperature responsiveness of hydrogels are crucial considerations for their role as condensing components. Nevertheless, there is a paucity of research on this topic in the current literature, and there are obvious gaps in the simulation of the structure of hydrogel networks formed by physical and chemical cross-linking. In this work, we employed MD simulations to investigate the effect of temperature and DOC on the water capture and release behavior of PNIPAM hydrogels. The conformational change of a PNIPAM-30mer polymer chain induced by the LCST was investigated from the nanoscale. Furthermore, the model of PNIPAM hydrogels cross-linked with BIS was built, the impact of temperature and DOC on the properties of thermosensitive hydrogels was investigated, including the diffusion coefficient of water, the number of hydrogen bonds between hydrogels and water, as well as the radial distribution function (RDF), and the pore size distribution (PSD).

2 Simulation Detail

2.1 PNIPAM-30mer Single Chain

The initial structure was prepared with Materials Studio [43]. Fig. 1a,b shows the polymerized repeating unit and the 3-D representations of the polymer chain. A simulation system with the three dimensions (9.6 nm × 9.6 nm × 9.6 nm) was built to investigate the temperature induced conformational change behavior of PNIPAM-30mer (Fig. 1c). Notably, the periodic boundary conditions were employed for the x, y, and z directions. Finally, a simulation system containing 31,740 water molecules and a PNIPAM-30mer chain was established.

2.2 Cross-Linked Hydrogel Preparation

As shown in Fig. 1d, R1 and R2 are the reaction sites of the pre-polymerized PNIPAM-5mer chains and BIS, respectively. The pre-polymerized PNIPAM-5mer chain and BIS provided four reaction sites and binding sites, respectively, with one BIS interconnects four chains (Fig. 1g). The Prepolymerized PNIPAM-5mer chains, BIS and water molecules produce different mixing systems depending on the water content (Fig. 1e). The PNIPAM hydrogels with different DOC values of 20 and 50%wt water content, which were 25%, 50%, 75% and 100%, were obtained by the cross-linking algorithm. According to previous studies, DOC was defined as the ratio of the number of cross-linking reactive atomic sites to the total number of N-isopropylacrylamide (NIPAM) reactive atomic sites present in the simulation system [33].

Materials Studio software was used for the dynamic cross-linking process, in which covalent bonds were formed between the pre-polymerized PNIPAM-5mer and the cross-linker. The initial mixing system consisted of the pre-polymerized PNIPAM-5mer chains, BIS, and water molecules with a NIPAM/BIS ratio of 4:1 for cross-linking PNIPAN hydrogels. This simulation system contains 200 NIPAM monomers, that is, 40 pre-polymerized PNIPAM-5mer chains. Then, water molecules were added according to different water contents to obtain different hydrogel systems. Hydrogel

systems with 25 and 50%wt of water contain 425 and 1700 water molecules, respectively. Before starting dynamic cross-linking, the system undergoes a sequence of equilibrium processes. Initially, the system energy is minimized through structure optimization. Subsequently, a 300 ps MD simulation is conducted in the NPT (constant number of particles N, constant pressure P, and constant temperature T) at 298 K. Finally, the system is heated to 698 K, maintained at a high temperature, and gradually cooled to a cross-linking temperature of 298 K for simulated annealing via MD simulation of the NVT (constant number of particles N, constant volume V, and constant temperature T) assembly.

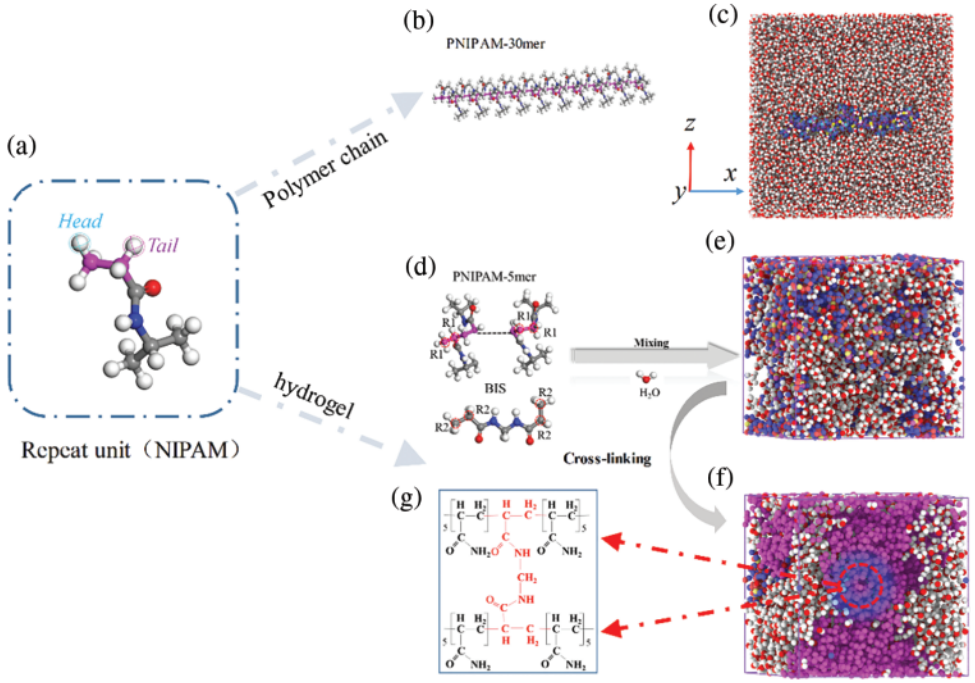

Figure 1: Diagram of the cross-linking. (a) Repeat unit. (b) 3-D representation of the PNIPAM-30mer. (c) PNIPAM-30mer system. (d) Pre-polymerized PNIPAM-5mer chain and BIS. (e) Mixing system. (f) Cross-linking PNIPAM hydrogel (DOC: 75%). (g) Form covalent crosslinking sites

The uncross-linked mixed systems were equilibrated to achieve the optimal structure for facilitating the cross-linking process, in this cross-linking algorithm [44], active atoms are specified to search for potential cross-linking partners within the search radius to form covalent bonds. The initial search radius is established at 4 Å, with the maximum search radius set at 9 Å. Following each iteration of the radius search, a supplementary NVT molecular dynamics simulation is conducted to alleviate any remaining stress, after which the search radius is incremented by 0.5 Å to repeat the search at the updated distance. Following the determination of the target bond length and bond force constants, a subsequent equilibration phase is conducted using the NVT ensemble. This iterative process continues until no suitable potential partner is identified within the designated search radius. There are two indicators that signify the completion of the cross-linking process: the attainment of the predetermined DOC and the reaching of the maximum search radius. The Condensed-phase Optimized Molecular Potentials for Atomistic Simulation Studies (COMPASSII) force field was employed for the dynamic cross-linking process. The Nose-Hoover thermostat was used to control the temperature and the Parrinello-Rahman barostat to regulate the pressure, respectively. The entirety of the system cross-linking and MD simulation procedure is depicted in Fig. 2. Following the acquisition

of the necessary hydrogel systems, subsequent simulations were conducted utilizing the LAMMPS (Large-scale Atomic/Molecular Massively Parallel Simulator) software package [45].

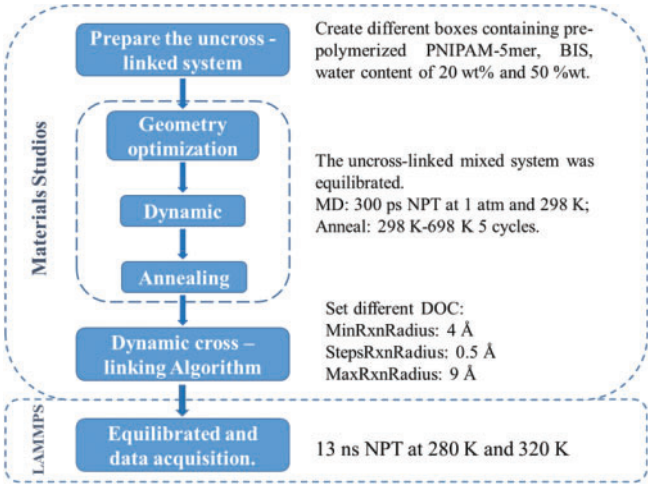

Figure 2: Flowchart of the cross-linking and MD process for hydrogel samples

2.3 MD Simulation Details

Both PNIPAM-30mer and hydrogels employed Consistent Valence Force Field (CVFF) force field, and rigid TIP3P model was used for the water, respectively. The interaction between components was described using Lennard-Jones 12-6 potential, $E = 4\varepsilon[(\sigma/r)^{12} - (\sigma/r)^{6}]$, where ε is the characteristic energy and σ is the van der Waals radius. And the arithmetic combining rule was used to determine the heteroatomic Lennard-Jones parameters. As shown in Table 1, the specific parameters of Lennard-Jones (LJ) potential of each atom of hydrogel. Besides, the real-space cutoff for the electrostatic potential and van der Waals forces was set to 10.0 Å. Long-range electrostatic and van der Waals interactions were computed using the particle-particle particle-mesh (PPPM) method with a Root Mean Square (RMS) accuracy of 10^{-4} [46]. The SHAKE algorithm was employed to constrain the bond lengths and angles of water molecules [47].

Table 1: The LJ parameters used in simulations for hydrogels

Atoms	Charge	ε (kcal/mol)	σ (Å)
C1	−0.1	0.0389999952	3.8754094636
C2	−0.2	0.0389999952	3.8754094636
H	0.1	0.0380000011	2.4499714540
N	0.38	0.1669999743	3.5012320066
O	−0.5	0.2280000124	2.8597848722
C3	−0.38	0.0389999952	3.8754094636
HN	0.28	0.0000000000	0.0000000000
C4	−0.3	0.0389999952	3.8754094636
C5	0	0.1599999990	3.4745050026

(Continued)

Table 1 (continued)

Atoms	Charge	ε (kcal/mol)	σ (Å)
O∗	−0.83	0.1020	3.1880
H∗	0.415	0	0

In the first part, PNIPAM-30mer single chain reproduced the temperature responsiveness of the material. The PNIPAM-30mer polymer chain was initially presented as an extended chain and then equilibrated under the NVT ensemble for 0.4 ns. Water molecules were added after minimization. Temperature equilibration was then performed in the NPT ensemble at 280 and 320 K and 1 bar for 0.4 ns. Data acquisition was performed using the production run in the NPT ensemble extended for 8 ns. A gradual heating simulation was then performed on the identical single chain system at a heating rate of 5 K/ns (from 280 to 320 K). The conformation changes of the PNIPAM-30mer chain, including End to End distance, Radius of gyration (Rg) and volume change of the polymer chain, were evaluated at a specific temperature and a dynamically changing temperature. The timestep for this part of the simulation is 2 fs.

In the second part, eight PNIPAM hydrogel systems were prepared with varying water content of 20 and 50%wt, and with DOC values of 25%, 50%, 75% and 100%, respectively. Each hydrogel system was equilibrated for 5 ns under the NPT ensemble at temperatures of 280 and 320 K. Subsequently, a molecular dynamics simulation process lasting 8 ns was conducted for data acquisition. The timestep for this part of the simulation is 1 fs. Throughout the entirety of the molecular dynamics process, the potential energy of both the hydrogel and water components was calculated, Equilibrium was considered to be reached when the potential energy exhibited stability. The MD simulation process was conducted following the attainment of system equilibrium, during which various pertinent parameters were assessed, including the quantity of hydrogen bonds, water diffusion coefficient, and PSD.

3 Results and Discussion

3.1 MD Simulation Details

The MD simulation of PNIPAM-30mer and water molecules were conducted at 320 and 280 K, which were above and below LCST (305 K), respectively. The temperature dependence of the End to End distance and the Rg of the polymer chain were also examined. The changes in End to End distance and Rg of PNIPAM-30mer in aqueous environments at two different temperatures are shown in Fig. 3a,b. The End to End distance and Rg of the polymer chain at 280 K fluctuated between 59 to 28 Å and 19 to 11 Å, respectively. However, the End to End distance and Rg reduced to 8 and 9 Å at 320 K. Furthermore, the shape and sizes of the polymer chain were significantly different at 280 and 320 K. Specifically, PNIPAM-30mer had an extended conformation below LCST, while the PNIPAM chain collapsed into a condensed conformation above LCST. These findings indicate that temperature changes substantially influence the conformational transition of the PNIPAM polymer chain. Fig. 4 shows the snapshot of PNIPAM-30mer during the MD simulation. At temperatures from 280 to 320 K, it can be seen that the polymer chain transforms from coil to globule.

Most previous studies focused on simulating the conformational changes of polymer chains at specific temperatures. In this study, the behavior of PNIPAM-30mer was simulated at gradual heating, and their dynamic evolution was assessed from 280 to 320 K. The Rg and End to End distance of the

polymer chain decreased with increasing temperature, indicating a transition conformation from coil to globule (Fig. 5). This conformational change was consistent with the conformational change at certain simulated temperatures (280 and 320 K) (Figs. 3 and 4).

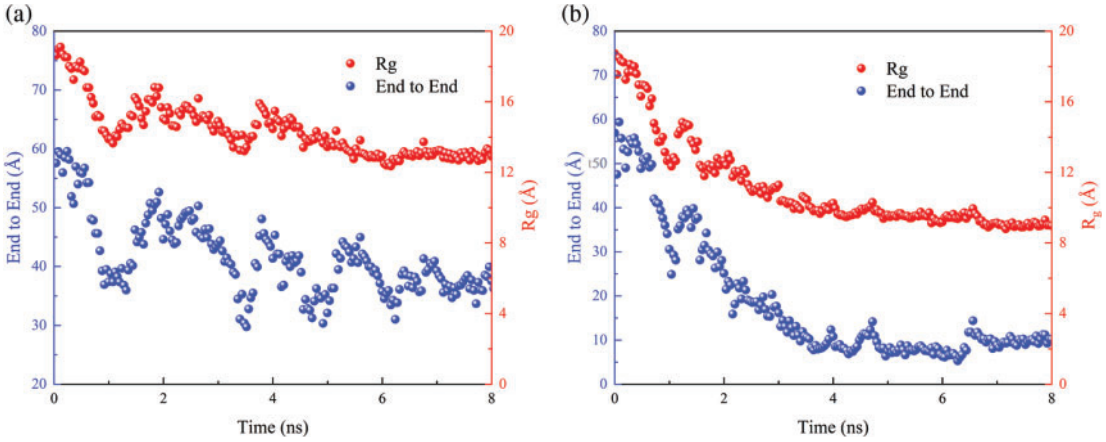

Figure 3: End to end distance (blue) and Rg of the PNIPAM-30mer chain (red) in 8 ns simulation time at 280 K (a) and at 320 K (b)

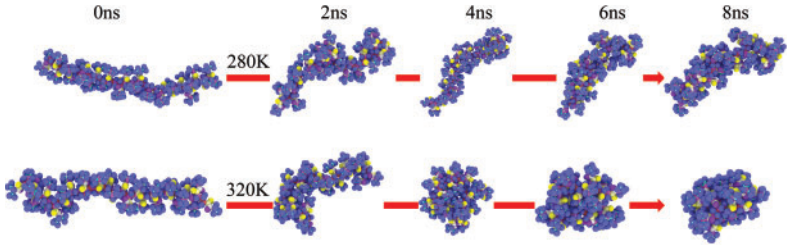

Figure 4: Snapshots of the hydrated PNIPAM-30mer chain at 280 K and at 320 K

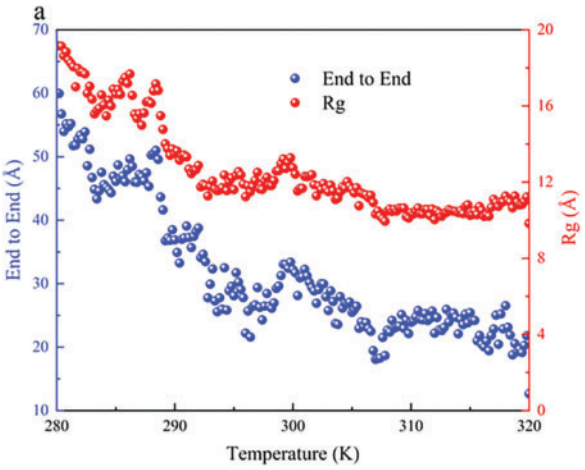

Figure 5: End to end distance (blue) and Rg (red) of the PNIPAM-30mer under gradual heating

The structural transition of PNIPAM-30mer was further investigated using the Voronoi tessellation method to analyze volume change data, revealing insights into the surface solvation state [48]. Voronoi tessellation partitions the volume of system into polyhedral cells, with each cell corresponding to an individual atom. The volume of each cell is defined by the set of points closest to the respective atom. The alterations in the volume of the polymer chain are shown in Fig. 6. The smaller volume of PNIPAM-30mer at 280 K can be attributed to its high hydrophilicity below LCST. This augmented hydrophilicity induces a greater propensity for the hydrophilic groups on the polymer chain to engage with water molecules, thereby facilitating the establishment of hydrogen bonds between the water and polymer chains. As a result, the hydrogen bonds promote the compaction of the polymer chain. The progressive volume changes of the polymer chain with increasing temperature are shown in Fig. 6. The polymer chain volume decreased with increasing temperature, possibly due to the heightened hydrophobic effect of the polymer chain, which increases water molecules surrounding the chain, thus diminishing its volume. We can see that the volume shows a decreasing trend. This observation contradicts the outcomes from the simulation results at two distinct temperatures, at 280 and 320 K. Consequently, it can be inferred that during the gradual heating process, the hydrophobic effect of the polymer chain becomes more pronounced with rising temperature, superseding the dominance of hydration. These findings indicate that the hydrophilic or hydrophobic characteristics of the polymer chain and the hydration between the polymer and water should be considered at certain temperatures, such as 280 K.

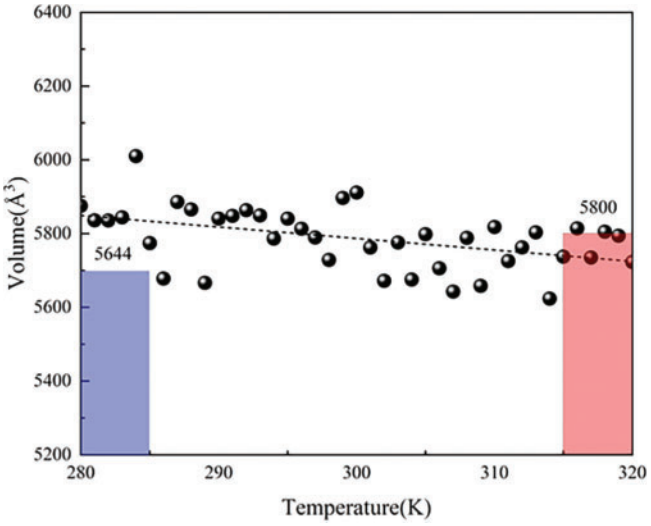

Figure 6: The volume of PNIPAM-30mer varies from 280 to 320 K

3.2 Cross-Linked Hydrogel System

In desalination systems, the current challenge should be to improve the liquefaction efficiency of vapor. Our research involves utilizing thermosensitive hydrogel as condensing elements in desalination systems, with a particular attention on the amount of fresh water captured. Specifically, the quantity of hydrated and free water each system at varying temperatures was obtained as illustrated in Fig. 7. The amount of free water captured serves as an indicator of the ability of thermosensitive hydrogel to release liquid water above its critical temperature. The cutoff distance for the first hydration shell was determined as 3.5 Å from the heavy atoms on the polymer surface based on previous theoretical study [49]. The figure illustrates that the number of water molecules decrease in the first hydration shell and

the free water increase above the LCST of 305 K. Furthermore, at water content of 20%wt, a trend is observed where the number of water molecules in the first hydration shell decreases as the temperature exceeds the critical temperature, leading to an increase in free water molecules. The corresponding changes in free water content for DOC values of 25%, 50%, 75%, and 100% are 16%, 6%, 14%, and 9%, respectively. Furthermore, at water content of 50%wt, the temperature responsiveness of the hydrogel is similarly demonstrated as the case of 20%wt, with corresponding free water increments of 7%, 9%, 10%, and 0% for DOC values ranging from 25% to 100%. At a water content of 20%wt, we can see that there is more free water with a DOC value of 25% and 75%. The hydrogel with 25% DOC exhibited lower levels of cross-linking pre-polymerized PNIPAM-5mer, resulting in increased release of free water and an unstable structure. It should be noted that 100% DOC value would lead to a worse temperature responsiveness, while lower DOC values result in instability of the hydrogel structure. In summary, among the four simulated cross-linking degrees, the DOC value of 75% is deemed optimal which can guide the preparation of thermosensitive hydrogels with both mechanical stability and high water-harvesting performance.

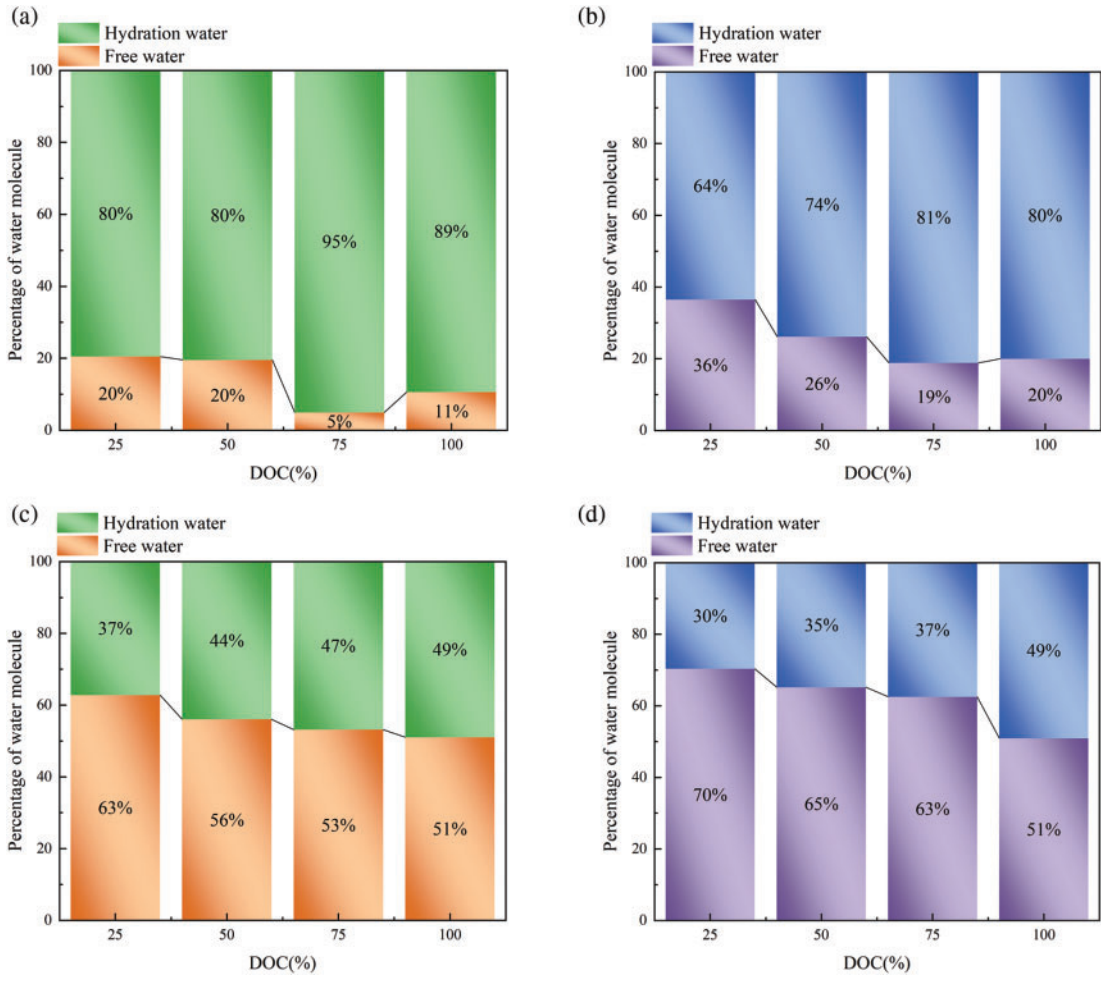

Figure 7: Number of free water and hydrated water with different DOC. (a, b) 20%wt water content at 280 and 320 K. (c, d) 50%wt water content at 280 and 320 K

Hydrogen bond plays a significant role in the evolution of dynamic results of thermosensitive hydrogels [50]. However, steric hindrances from the isopropyl group may limit the development of hydrogen bond interactions between the NH group and water molecules, resulting in insignificant contributions from NH-water pairs [51]. Consequently, only the average number of distinct hydrogen bonds between polar groups (=O) and water molecules in the hydrogel was quantified over the course of an 8 ns simulation. In this study, hydrogen bonds were defined based on specific criteria: a pair was considered hydrogen-bonded if the donor-acceptor distance was less than 3.6 Å, the hydrogen-acceptor distance was less than 2.45 Å, and the angle between the donor-hydrogen vector and the donor-acceptor vector was less than 30° [52]. As depicted in Fig. 8, the data indicates that at water contents of 20 and 50%wt, the average number of hydrogen bonds at 280 K exceeds that at 320 K for all levels of cross-linking. The decrease in the number of hydrogen bonds between hydrogels and water at higher temperatures suggests that the hydrophobic nature of the hydrogels increased at 320 K. The stability of the hydrogen bonding network was compromised above LCST, resulting in the loss of favorable interactions with adjacent water molecules, thus leading to the collapse of the hydrogels. In contrast, the hydrogen bond strength was significantly increased below the LCST, thus promoting the hydrophilic behavior of hydrogels. It is evident that a high temperature could result in the release of water molecules from the hydrogel, leading to their transformation into free water. The simulation results further illustrate that, at DOC value of 75%, the most hydrogen bonds are observed at 280 K under both water content conditions, suggesting a better hydrophilicity of the hydrogel at this particular level of cross-linking.

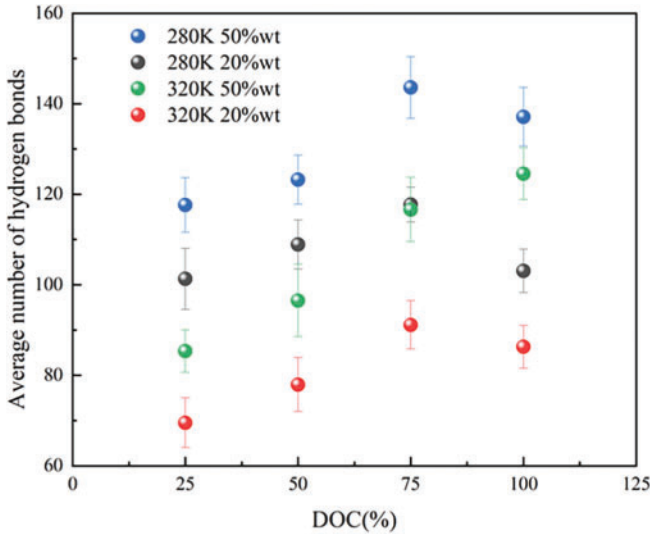

Figure 8: The average number of hydrogen bonds of different DOC at 280 and 320 K

The RDF refers to the coordinates of a given particle and describes the average probability of finding a particle at a given distance relative to a reference particle, compared to the average probability of finding a particle at that distance in an ideal gas. Specifically, RDF g(r) reflects the average density from one particle to another particle in a shell at a distance of r. To investigate the impact of DOC on the temperature responsiveness of PNIPAM hydrogel, the RDF of water oxygen (O_w) and amide oxygen (O_p) were also computed. The simulation results depicted in Fig. 9 illustrate variations at different temperatures and DOC. The findings suggest that an elevation in temperature leads to a reduction in the level of organization between the hydrogel and water molecules, as evidenced by a

decrease in the peak value, indicating the expulsion of water from the hydrogel structure. Fig. 9a and b shows the RDF between hydrogel oxygen and water oxygen at 280 and 320 K for 20%wt water content, respectively. The simulation results illustrate a decrease for the peak value of RDF as the temperature surpasses the LCST. The maximum peak value at DOC = 75% in Fig. 9a aligns with the hydrogen bond findings in Fig. 8. The peak values for different DOC (25, 50, 75, 100) were observed to decrease as the increased temperature for a water content of 50 and 20%wt. Interestingly, at a DOC of 100%, the peak value increased compared to 280 K, indicating that a higher level of cross-linking does not necessarily result in improved water release performance of the hydrogel.

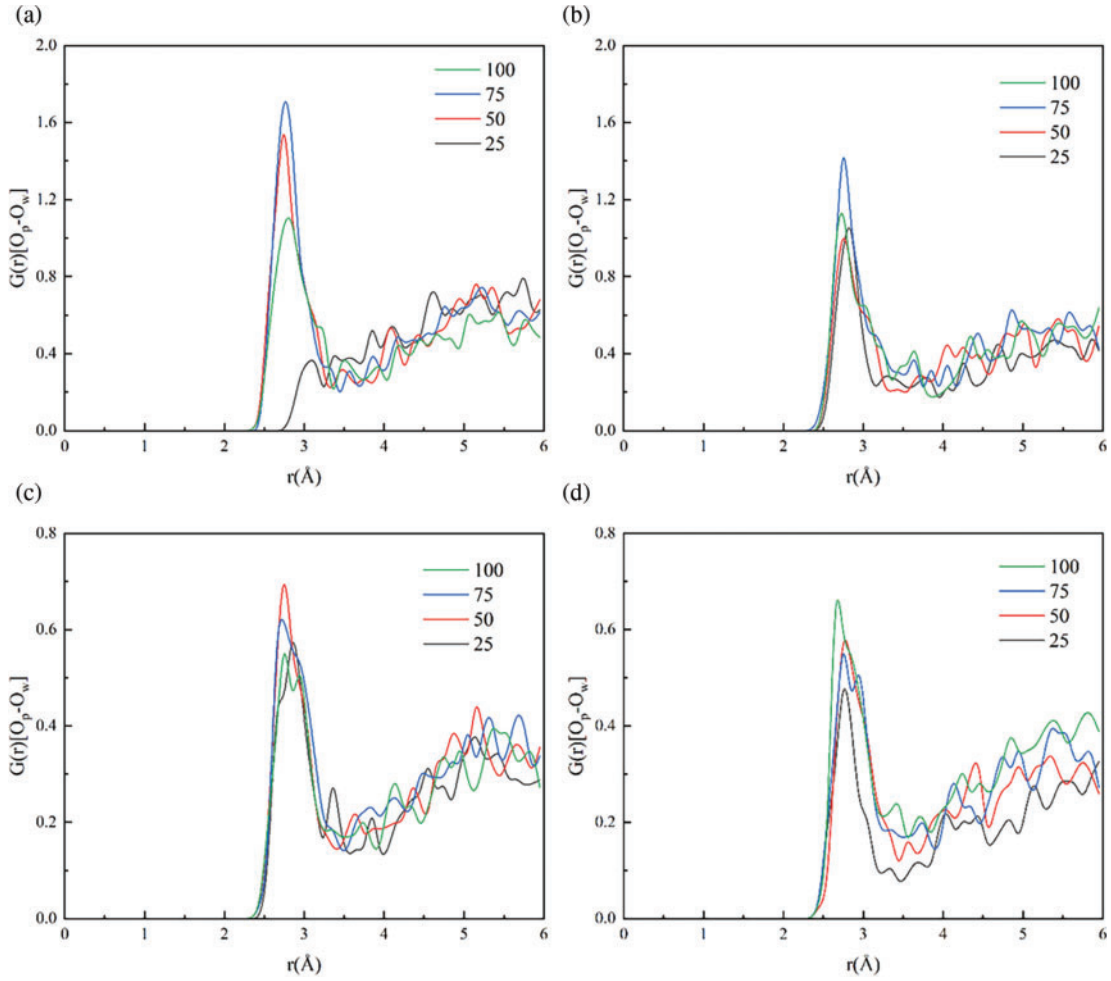

Figure 9: RDF of oxygen in hydrogel (O_p) and oxygen in water (O_w) at two water content for (a, b) 20%wt; (c, d) 50%wt; 280 K (left), 320 K (right)

Water release behavior is closely related to the diffusion of water molecules in thermosensitive gel. Mean squared displacements (MSD) can be accurately determined over time through MD simulations. The value of MSD at a specific time, equivalent to a designated experimental resolution, can be tracked in relation to temperature. The calculation formula for MSD is as follows:

$$MSD = < |r(t) - r(0)|^2 > \quad (1)$$

The relationship between MSD and diffusion coefficient D is as follows:

$$D = \lim_{t \to \infty} \frac{1}{6t} < |r(t) - r(0)|^2 > \quad (2)$$

Hence, the diffusion coefficient of water can be determined through analysis of the MSD diagram. Fig. 10 and Table 2 depict the MSD and diffusion coefficient of water molecules.

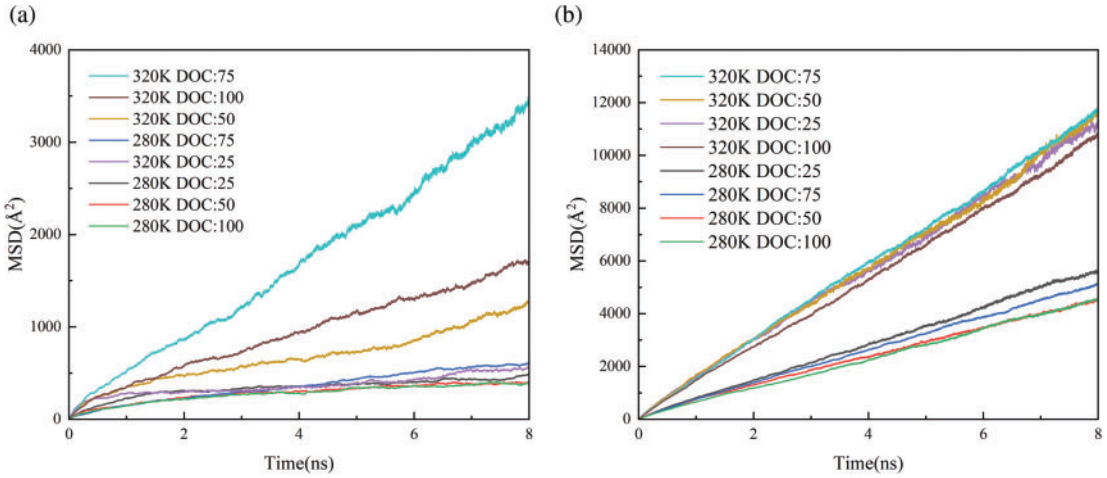

Figure 10: Temperature dependence of MSD calculated for water. (a) 20%wt water content. (b) 50%wt water content

Table 2: The diffusion coefficient of water molecules

Water content: 20%wt			Water content: 50%wt
Diffusion coefficient (Å²/fs)	Temp (K)	DOC (%)	Diffusion coefficient (Å²/fs)
0.66E−5 ± 0.28E−7	280	25	1.14E−4 ± 0.36E−7
0.60E−5 ± 0.21E−7		50	0.91E−4 ± 0.31E−7
1.13E−5 ± 1.13E−8		75	0.54E−4 ± 0.23E−7
0.61E−5 ± 0.19E−7		100	0.91E−4 ± 0.33E−7
0.72E−5 ± 0.47E−8	320	25	2.28E−4 ± 0.82E−7
0.21E−4 ± 0.34E−8		50	2.32E−4 ± 1.15E−7
0.69E−4 ± 0.40E−7		75	2.38E−4 ± 0.55E−7
0.32E−4 ± 0.23E−7		100	2.18E−4 ± 0.55E−7

It is evident that at the temperature of 320 K, the diffusion coefficient of water increases. For instance, at a cross-linking degree of 75% and temperatures of 280 and 320 K, the diffusion coefficients of water are 1.13×10^{-5} Å²/fs and 0.69×10^{-4} Å²/fs for 20%wt water content, respectively. It is observed that at temperatures exceeding the LCST, the diffusion coefficient of water increases, suggesting faster migration of water within the hydrogel. This results in improved water release performance of the thermosensitive hydrogel, leading to expulsion of water from the skeleton structure of the hydrogel. Furthermore, it is obvious that the diffusion coefficient of water is maximized at a temperature of 320 K and a cross-linking degree of 75% for all water contents. It can be summed up that among the

four levels of cross-linking, the hydrogel with the 75% DOC value exhibits the most optimal water release performance.

PSD is referring to describe the distribution of aperture material at various levels based on quantity or volume percentage. The calculation of PSD for porous materials is commonly utilized to characterize their properties [53]. PSD serves as a valuable indicator for evaluate the adsorption and release capabilities of hydrogels. Here, we use Poreblazer, a tool for calculating material structure, to calculate the PSD of each cross-linking hydrogel system [54]. Poreblazer detects the pore size of a porous material by simulating a probe particle moving through its structure. The diameter of the probe particle can be a variable parameter used to simulate the size of different molecules. The probe particles move along multiple paths, and by calculating the maximum passable diameter at each point, the maximum and minimum apertures encountered by the probe particles of different sizes on all paths are counted to generate a local aperture distribution. The PSD calculations for each hydrogel system under varying temperature and water content conditions are depicted in Fig. 11. It should be particularly pointed out that the calculation of PSD was performed after the completion of the 8 ns simulation, and only the hydrogel skeleton structure was considered, ignoring the presence of water. Because of the complexity and randomness of the cross-linking process of hydrogel, the cross-linking system model has its unique pore size distribution, which is difficult to normalize. And for thermosensitive gels, it is expected that when the simulated temperature is higher than LCST, the collapse of the gel skeleton structure due to the release of water will lead to larger pores in the simulated cells [38]. Based on the data presented in Fig. 11a,b, it is evident that at a water content of 20%wt, the PSD of thermosensitive gel systems with DOC of 50% and 75% is primarily concentrated within the range of 2.5∼4 Å and 2.2∼4.5 Å at a temperature of 280 K. Upon reaching a temperature above the LCST of 320 K, the pore size of the hydrogels systems increases. Specifically, at the DOC of 50%, there is a significant increase in pore size, with a peak observed between 15 and 15.8 Å. Similarly, at the DOC of 75%, the pore size also increases to a range of 2.5∼9.5 Å. The results indicate that at the DOC of 25% and 100%, the pore size distribution at 280 K shows the presence of voids for both large and small pores, with no clear pattern. However, at 320 K, an increase in the number of large pores is observed. Specifically, at a cross-linking degree of 100% and 320 K, a peak in the distribution occurs between pore sizes 15 and 17 Å. Similar trends are observed in the pore size distribution at 50%wt water content, with an increase in the number of large pores at elevated temperatures.

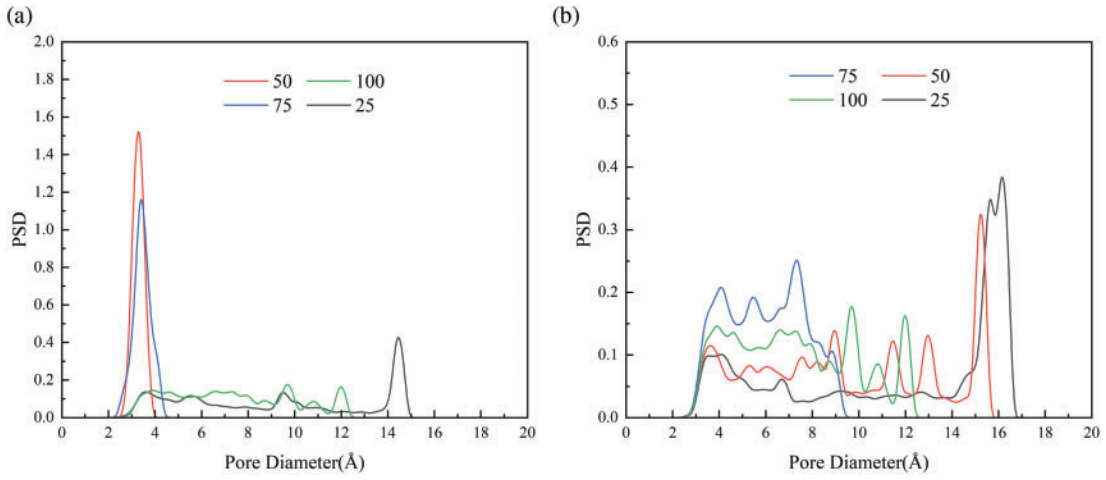

Figure 11: (Continued)

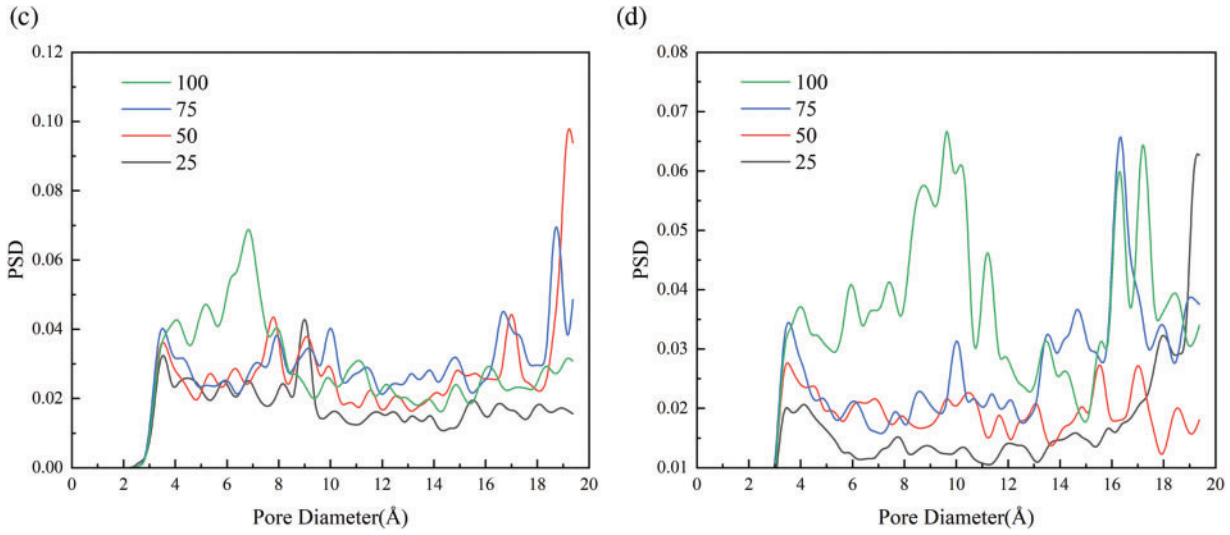

Figure 11: PSD for (left) 280 K and (right) 320 K hydrogel at different water contents, 20%wt (a, b), 50%wt (c, d)

4 Conclusion

In this study, molecular dynamics simulations were used to explore the dynamic characteristics of individual PNIPAM-30mer chain and hydrogel systems below and above the LCST. First of all, we verified that the free PNIPAM chain significantly responded to temperature changes, consistent with previous studies. By a series of statistics including the Rg and End to End distance, the polymer chain is temperature responsiveness and will undergo coil to globule transition above the LCST. Secondly, a simulation study of cross-linking thermosensitive hydrogels reveals the release of free water within the hydrogel network upon reaching temperatures above the LCST. Furthermore, the impact of varying degrees of cross-linking on the thermal responsiveness of PNIPAM hydrogels was examined. Parameters such as the quantity of expelled free water, hydrogen bonds, Rg, diffusion coefficient and PSD were analyzed to assess the water release characteristics of the cross-linking thermosensitive hydrogels. Among the simulated cross-linking degrees, the thermosensitive hydrogels exhibited optimal temperature responsiveness and structural stability at a cross-linking degree of 75%.

In conclusion, the feasibility of the principle was verified by the simulation of single chain, and the practicality of the material was verified by cross-linking thermosensitive hydrogels. Moreover, findings showed that PNIPAM hydrogel is a viable mobile freshwater material. Porous thermosensitive gels are potential condensing components in solar thermal desalination systems due to their flexible thermal response. Nonetheless, further studies should assess the adsorption-condensation behavior of thermal gels and explore viable thermal design approaches for the dynamic water capture-release process and adaptive operation of condensing components in photothermal desalination systems.

Acknowledgement: None.

Funding Statement: This work was supported by National Natural Science Foundation of China (No. 52206073), Fundamental Research Funds for the Central Universities (No. 3132023119), and Guangdong Basic and Applied Basic Research Foundation (Nos. 2024A1515011379 and 2023A1515110613).

Author Contributions: The authors confirm contribution to the paper as follows: study conception and design: Dong Niu, Mu Du; data collection: Hongtao Gao, Xianzhi Chen; analysis and interpretation of results: Xianzhi Chen; draft manuscript preparation: Dong Niu, Xianzhi Chen. All authors reviewed the results and approved the final version of the manuscript.

Availability of Data and Materials: Data available on request from the authors.

Ethics Approval: Not applicable.

Conflicts of Interest: The authors declare no conflicts of interest to report regarding the present study.

References

1. Ghasemi H, Ni G, Marconnet AM, Loomis J, Yerci S, Miljkovic N, et al. Solar steam generation by heat localization. Nat Commun. 2014;5:4449. doi:10.1038/ncomms5449.
2. Luo X, Shi J, Zhao C, Luo Z, Gu X, Bao H. The energy efficiency of interfacial solar desalination. Appl Energy. 2021;302:117581. doi:10.1016/j.apenergy.2021.117581.
3. Ni G, Zandavi SH, Javid SM, Boriskina SV, Cooper TA, Chen G. A salt-rejecting floating solar still for low-cost desalination. Energy Technol Environ. 2018;11(6):1510–9. doi:10.1039/C8EE00220G.
4. Zhu K, Li S, Pilon L. Light transfer through windows with external condensation. J Quant Spectrosc Radiat Transfer. 2018;208:164–71. doi:10.1016/j.jqsrt.2018.01.019.
5. Jani HK, Modi KV. Experimental performance evaluation of single basin dual slope solar still with circular and square cross-sectional hollow fins. Sol Energy. 2019;179:186–94. doi:10.1016/j.solener.2018.12.054.
6. Mulroe MD, Srijanto BR, Ahmadi SF, Collier CP, Boreyko JB. Tuning superhydrophobic nanostructures to enhance jumping-droplet condensation. ACS Nano. 2017;11(8):8499–510. doi:10.1021/acsnano.7b04481.
7. Dai ZS, Zhang Y, Wang S, Nawaz K, Jacobi A. Falling-film heat exchangers used in desalination systems: a review. Int J Heat Mass Transfer. 2022;185:122407. doi:10.1016/j.ijheatmasstransfer.2021.122407.
8. Cho E, Lee H, Kang M, Jung D, Lee G, Lee S, et al. A neural network model for free-falling condensation heat transfer in the presence of non-condensable gases. Int J Therm Sci. 2022;171:107202. doi:10.1016/j.ijthermalsci.2021.107202.
9. Lutolf MP, Hubbell JA. Synthetic biomaterials as instructive extracellular microenvironments for morphogenesis in tissue engineering. Nat Biotechnol. 2005;23(1):47–55. doi:10.1038/nbt1055.
10. Peppas NA, Hilt JZ, Khademhosseini A, Langer R. Hydrogels in biology and medicine: from molecular principles to bionanotechnology. Adv Mater. 2006;18(11):1345–60. doi:10.1002/adma.200501612.
11. Maurdev G, Millington KRJ. Potential for desalination using lower critical solution temperature polymers: concentration of salt solutions by pluronic PE6200. Appl Polym Sci. 2009;113(4):2346. doi:10.1002/app.30309.
12. Lin ST, Yu H, Zhang T, Parada GA, Koo H, Yu C, et al. Stretchable hydrogel electronics and devices. Adv Mater. 2016;28(22):4497–505. doi:10.1002/adma.201504152.
13. Nisar S, Dastgeer G, Shahzadi M, Shahzad ZM, Elahi E, Irfan A, et al. Gate-assisted $MoSe_2$ transistor to detect the streptavidin via supporter molecule engineering. Mater Today Nano. 2023;24:2588–8420. doi:10.1016/j.mtnano.2023.100405.
14. Lu HY, Shi W, Guo Y, Guan WX, Lei CX, Yu GH. Materials engineering for atmospheric water harvesting: progress and perspectives. Adv Mater. 2022;34(12):2110079. doi:10.1002/adma.202110079.
15. Xu J, Li T, Yan T, Wu S, Wu MQ. Ultrahigh solar-driven atmospheric water production enabled by scalable rapid-cycling water harvester with vertically aligned nanocomposite sorbent. Energy Environ Sci. 2021;14:5979–94. doi:10.1039/D1EE01723C.

16. Shi Y, Ilic O, Atwater HA, Greer JR. All-day fresh water harvesting by microstructured hydrogel membranes. Nat Commun. 2021;12(1):1–10. doi:10.1038/s41467-021-23174-0.
17. Li X, Zhang Z, Xie Z, Guo X, Yang T, Li Z, et al. High performance and self-humidifying of novel cross-linked and nanocomposite proton exchange membranes based on Sulfonated Polysulfone. Nanomaterials. 2022;12(5):841. doi:10.3390/nano12050841.
18. Yu W, Zhou Y, Li ZD, Zhu DH, Wang LL, Lei QX, et al. When thermochromic material meets shape memory alloy: a new smart window integrating thermal storage, temperature regulation, and ventilation. Appl Energy. 2024;372:0306–2619. doi:10.1016/j.apenergy.2024.123821.
19. Halperin A, Kroger M, Winnik FM. Poly(*N*-isopropylacrylamide) phase diagrams: fifty years of research. Int Ed. 2015;54(51):15342–67. doi:10.1002/anie.201506663.
20. Lopez CG, Richtering W. Does Flory-Rehner theory quantitatively describe the swelling of thermoresponsive microgels. Soft Matter. 2017;13(44):8271–80. doi:10.1039/c7sm01274h.
21. Lorbeer L, Alaghemandi M, Spohr E. Molecular dynamics studies of poly(N-isopropylacrylamide) end-grafted on the surfaces of model slab pores. J Mol Liq. 2014;189:57–62. doi:10.1016/j.molliq.2013.05.022.
22. Tavagnacco L, Chiessi E, Zaccarelli E. Molecular insights on poly(*N*-isopropylacrylamide) coil-to-globule transition induced by pressure. Phys Chem Chem Phys. 2021;23(10):5984–91. doi:10.1039/D0CP06452A.
23. Saleki O, Moosavi A, Hannani SK. Friction reduction in a nanochannel with grafted poly(N-isopropylacrylamide) oligomers: a molecular dynamics study. Phys Fluids. 2021;33(5):052004. doi:10.1063/5.0050658.
24. Gammas S, Suzuki K, Sone C, Sakurai Y, Kataoka K, Okano T. Thermoresponsive polymer nanoparticles with a core-shell micelle structure as sitespecific drug carriers. J Control Release. 1997;97:157–64. doi:10.1016/S0168-3659(97)00040-0.
25. Wei H, Zhang XZ, Zhou Y, Cheng SX, Zhuo RX. Self-assembled thermoresponsive micelles of poly(*N*-isopropylacrylamide-*b*-methyl methacrylate). Biomaterials. 2006;27(9):2028–34. doi:10.1016/j.biomaterials.2005.09.028.
26. Bai X, Bao Z, B. S, Li Y, Yu X, Hu S, et al. Chitosan-based thermo/pH double sensitive hydrogel for controlled drug delivery. Macromol Biosci. 2018;18(3):1700305. doi:10.1002/mabi.201700305.
27. Hu W, Wang Z, Xiao Y, Zhang S, Wang J. Advances in crosslinking strategies of biomedical hydrogels. Biomater Sci. 2019;7(3):843–55. doi:10.1039/C8BM01246F.
28. Zhang X, Shen W, Dou J, Meng Y, Fang S, Liu R. Enhanced mechanical properties and self-healing behavior of PNIPAM nanocomposite hydrogel by using POSS as a physical crosslinker. J Appl Polym Sci. 2020;137(12):48486. doi:10.1002/app.48486.
29. Tuncaboylu DC, Argun A, Algi MP, Okay O. Autonomic self-healing in covalently crosslinked hydrogels containing hydrophobic domains. Polymer. 2013;54(23):6381–8. doi:10.1016/j.polymer.2013.09.051.
30. Wu C. Cooperative behavior of poly(vinyl alcohol) and water as revealed by molecular dynamics simulations. Polymer. 2010;51(19):4452–60. doi:10.1016/j.polymer.2010.07.019.
31. Demir B, Walsh TR. A robust and reproducible procedure for cross-linking thermoset polymers using molecular simulation. Soft Matter. 2016;12(8):2453–64. doi:10.1039/C5SM02788H.
32. An M, Demir B, Wan X, Meng H, Yang N, Walsh TR. Predictions of thermomechanical properties of cross-linked polyacrylamide hydrogels using molecular simulations. Adv Theory Simul. 2019;2:1800153. doi:10.1002/adts.201800153.
33. Jang SS, Goddard WA, Kalani MYS. Mechanical and transport properties of the poly(ethylene oxide)-poly(acrylic acid) double network hydrogel from molecular dynamic simulations. J Phys Chem B. 2007;111(7):1729–37. doi:10.1021/jp0656330.

34. Lee SG, Brunello GF, Jang SS, Bucknall DG. Molecular dynamics simulation study of P (VP-co-HEMA) hydrogels: effect of water content on equilibrium structures and mechanical properties. Biomaterials. 2009;30:6130. doi:10.1016/j.biomaterials.2009.07.035.
35. Tavagnacco L, Chiessi E, Zanatta M, Orecchini A, Zaccarelli E. Water-polymer coupling induces a dynamical transition in microgels. J Phys Chem Lett. 2019;10(4):870–6. doi:10.1021/acs.jpclett.9b00190.
36. Zanatta M, Tavagnacco L, Buratti E. Atomic scale investigation of the volume phase transition in concentrated PNIPAM microgels. J Chem Phys. 2020;152(20):204904. doi:10.1063/5.0007112.
37. Tamai Y, Tanaka H, Nakanishi K. Molecular dynamics study of polymer-water interaction in hydrogels. 1. Hydrogen-bond structure. Macromolecules. 1996;29(21):6750–60. doi:10.1021/ma951635z.
38. Deshmukh S, Mooney DA, MacElroy JMD. Molecular simulation study of the effect of cross-linker on the properties of poly(*N*-isopropyl acrylamide) hydrogel. Mol Simulat. 2011;37(10):846–54. doi:10.1080/08927022.2011.566608.
39. Lehmann M, Krause P, Miruchna V, Klitzing R. Tailoring PNIPAM hydrogels for large temperature-triggered changes in mechanical properties. Coll Polym Sci. 2019;297(4):633–40. doi:10.1007/s00396-019-04470-0.
40. Kratz K, Lapp A, Eimer W, Hellweg T. Volume transition and structure of triethyleneglycol dimethacrylate, ethylenglykol dimethacrylate, and *N,N′*-methylene bis-acrylamide cross-linked poly(*N*-isopropyl acrylamide) microgels: a small angle neutron and dynamic light scattering study. Colloid Surf A. 2002;197:55–67.
41. Jang JW, Park JH. Preparation and characterization of thermoresponsive poly(N-isopropylacrylamide-co-N-isopropylmethacrylamide) hydrogel materials for smart windows. J Appl Polym Sci. 2020;138(6):49788. doi:10.1002/app.49788.
42. Chen XZ, Niu D, Gao HT. Deswelling mechanisms of PNIPAM grafted in nanochannels: a molecular dynamics simulation study. Langmuir. 2024;40(14):7692–700. doi:10.1021/acs.langmuir.4c00381.
43. Liu SY, Guo YX, Jiang YF, Gong YG, Hu QZ, Yu L. Single-chain conjugated polymer guests confined inside Metal-Organic Frameworks (MOFs): boosting the detection and degradation of a sulfur mustard simulant. Anal Chem. 2024;96(6):2333–40. doi:10.1021/acs.analchem.3c03588.
44. Shokuhfar A, Arab B. The effect of cross linking density on the mechanical properties and structure of the epoxy polymers: molecular dynamics simulation. J Mol Model. 2013;19(9):3719–31. doi:10.1007/s00894-013-1906-9.
45. Plimpton S. Fast parallel algorithms for short-range molecular dynamics. J Comput Phys. 1995;117(1):1–19. doi:10.1006/jcph.1995.1039.
46. Hockney RW, Goel SP, Eastwood JW. Quiet high-resolution computer models of a plasma. J Comput Phys. 1974;14(2):148–58. doi:10.1016/0021-9991(74)90010-2.
47. Alaghemandi M, Leroy F, Muller-Plathe F, Bohm MC. Thermal rectification in nanosized model systems: a molecular dynamics approach. Phys Rev B: Condens Matter Mater Phys. 2010;81(12):125410. doi:10.1103/PhysRevB.81.125410.
48. Isele-Holder RE, Rabideau BD, Ismail AE. Definition and computation of intermolecular contact in liquids using additively weighted voronoi tessellation. J Phys Chem A. 2012;116:4657– 66. doi:10.1021/jp3021886.
49. Conner BN, Yoon C, Dickerson JL, Dickerson RE. Helix geometry and hydration in an A-DNA tetramer. J Mol Biol. 1984;174(18):663. doi:10.1016/0022-2836(84)90089-5.
50. Ahmed Z, Gooding EA, Pimenov KV, Wang LL, Asher SA. UV resonance raman determination of molecular mechanism of poly(*N*-isopropylacrylamide) volume phase transition. J Phys Chem B. 2009;113(13):4248–56. doi:10.1021/jp810685g.
51. Lee SG, Pascal TA, Koh W, Brunello GF, Goddard WA, Jang SS. Deswelling mechanisms of surface-grafted Poly(NIPAAM) brush: molecular dynamics simulation approach. J Phys Chem C. 2012;116(30):15974–85. doi:10.1021/jp301610b.

52. Luzar A, Chandler D. Structure and hydrogen bond dynamics of water-dimethyl sulfoxide mixtures by computer simulations. J Phys Chem. 1993;98:8160–73. doi:10.1063/1.464521 .
53. Bhattacharya S, Gubbins KE. Fast method for computing pore size distributions of model materials. Langmuir. 2006;22(18):7726–31. doi:10.1021/la052651k.
54. Sarkisov L, Bueno-Perez R, Sutharson M, Fairen-jimenez D. Material informatics with PoreBlazer v4.0 and CSD MOF database. Chem Mater. 2020;32(23):9849–67. doi:10.26434/chemrxiv.12923558.